Journal of Analytical and Applied Pyrolysis 110 (2014) 424–429

Contents lists available at ScienceDirect

Journal of Analytical and Applied Pyrolysis

journal homepage: www.elsevier.com/locate/jaap

Temperature dependence of aspen torrefaction kinetics

Jordan Klinger[a,*], Bethany Klemetsrud[b], Ezra Bar-Ziv[a], David Shonnard[b,c]

[a] Department of Mechanical Engineering-Engineering Mechanics, Michigan Technological University, Houghton, MI 49931, USA
[b] Department of Chemical Engineering, Michigan Technological University, Houghton, MI 49931, USA
[c] Sustainable Futures Institute, Michigan Technological University, Houghton, MI 49931, USA

ARTICLE INFO

Article history:
Received 12 June 2014
Accepted 20 October 2014
Available online 29 October 2014

Keywords:
Torrefaction
Kinetic model
Temperature dependence
Arrhenius behavior

ABSTRACT

Torrefied biomass provides opportunities for an alternative, renewable fuel in the energy market. Much work on torrefaction is based on weight loss transients without much insight into the evolution of volatile species. A previous model from our group has been developed that predicts the degradation of raw biomass into specific chemical species during torrefaction (water, acetic acid, carbon monoxide, carbon dioxide, formic acid and furfural) in three consecutive reaction steps. The goal of this work is to understand how the kinetics of torrefaction change with temperature. Kinetic parameters for aspen wood were obtained for the first 90 min of 260–300 °C (1000 °C/s) torrefaction. The pre-exponential factors were 3.32E9, 1.43E11, and 2.08E14 min^{-1}, and the activation energies 1.05E2, 1.27E2, and 1.72E2 kJ/mol for the three reactions. Kinetic parameters found correspond well to similar values from global weight loss studies, and suggest that increased torrefaction severity leads to progressively more recalcitrant forms of torrefied biomass. These continuous production traces for the volatile organic species yield insight into torrefaction, and require careful consideration of torrefaction time and temperature to design the desired solid fuel product.

© 2014 Elsevier B.V. All rights reserved.

1. Introduction

Currently 42% of the electricity generated in the United States comes from coal combustion [1,2]. Coal is known to produce one-third of the CO_2 emissions in the United States and releases other harmful pollutants such as CO, SO_x, NO_x, particulates, and mercury. Because of the growing concern of global warming, the need to find renewable CO_2 neutral feedstock is immediate. Biocoal (or torrefied biomass) [3–6] can be an immediate solution in coal utility boilers. This renewable fuel can be used as a drop-in replacement for coal firing due to its high energy density, similar properties to coal, low emissions and potential for CO_2 neutrality [3,6,7].

Biocoal is produced from the torrefaction of biomass, at temperatures from 200 to 300 °C in an oxygen free environment. During torrefaction, mostly the hemicellulose portion of the biomass degrades through a complex coupled chemical-kinetic-heat-and-mass-transfer process [7–9]. There are small contributions from cellulose and lignin during this process; with the contribution of cellulose increasing significantly at temperatures above 300 °C [8,10]. When the biomass is heated up quickly in an inert atmosphere, biomass is dehydrated, the viscoelastic properties are changed, and the calorific value increases [6,11]. In addition, the energy requirements to reduce the size biocoal is substantially smaller, up to an order of magnitude, when compared to raw biomass [4,5,7,12,13]. Biocoal is then able to be a drop-in replacement for pulverized coal.

In order to have a better control of the torrefaction process and develop more efficient reactors for biocoal production, the torrefaction of biomass and the kinetics of species evolution, and changes in the residual biomass need to be better understood. Much gravimetric work has been done to model changes during torrefaction such as parallel reaction [7,14–16] and consecutive reactions models [10,17–20]. These models are useful for targeting throughput in equipment design, but provide little insights into the value-added benefits of torrefaction such as the improved fuel and physical properties over raw biomass mentioned above. A detailed understanding of the feedstock degradation during the torrefaction process, or the gas species evolution, is necessary for prediction of product quality changes with reaction conditions.

One specific approach to modeling torrefaction kinetics is to develop equations around weight loss data. One such model that is well accepted in literature is the two stage degradation of hemicellulose (xylans) developed by Di Blasi and Lanzetta [17]. This two stage model first degrades to a solid intermediate through rate constant k_1, and volatiles through kv_1, followed by a sequential step to torrefied biomass through k_2 and more volatile products through

---

[*] Corresponding author. Tel.: +1 616 430 094; fax: +1 906 487 2822.
E-mail address: jlklinge@mtu.edu (J. Klinger).

http://dx.doi.org/10.1016/j.jaap.2014.10.008
0165-2370/© 2014 Elsevier B.V. All rights reserved.

kv_2. This model predicts one stage of degradation at early times, and one stage for degradation over long processing times. The rate constants for each stage are also combined to give a global rate constant for that step ($k_1 = k_B + kv_1$, $k_2 = k_C + kv_2$). This was further developed by Di Blasi and Branca in subsequent years to include a similar third degradation stage (constants now k_B and kv_1, k_D and kv_2, and k_C and kv_3, respectively) when whole wood species (beech) were studied instead of xylans [21,22]. Further, these rate constants were combined to predict the pseudo-reactions where k_1 is the sum of the constants for volatile production and the production of the solid intermediate ($k_1 = kv_1 + k_B$) in reaction one. The six rate coefficients were therefore combined and analyzed as three global constants ($k_1 = kv_1 + k_B$, $k_2 = kv_2 + k_D$, $k_3 = kv_3 + k_C$) from 528 K to 584 K (6000 s), and 573 K to 708 K (up to 2000 s). The first reaction (k_1) was reported to dominate from 528 K to 593 K, the second (k_2) from 528 K to 708 K, and the third (k_3) from 603 K to 708 K. While these models may be convenient for estimating material throughput in equipment design, they do not provide any process insight into product quality, or any information on a chemical level.

Several studies have investigated modeling of torrefaction and coupling information about volatile species evolution [10,18–20,23,24]. Prins et al. studied the torrefaction of willow over 225–300 °C using the Di Blasi and Lanzetta model discussed above [10]. This was quickly followed by a subsequent study investigating the product distribution that is observed [23]. These were later combined to accurately predict the volatile product evolution over a range of temperatures and times [19]. More recently, Nocquet et al., took a similar approach using beechwood, cellulose, lignin, and xylan standards [20,24]. In the kinetic study, the two-stage Di Blasi and Lanzetta model was used to model the decomposition of the cellulose, hemicellulose, and lignin fractions of the biomass, with a stoichiometry parameter for the production of the respective volitile species [20]. With a correction facor to account for the interaction of the related consituents of virgin wood, they were able to accurately predict the volitile evolution at descite points, and also match a continuious mass loss signal. In order to move beyond a descrete point understanding of volitile torrefaction species, however, our group previously investigated a model based strictly around gas-phase species kinetics [18].

The previous study predicts the first 90 min of torrefaction at 300 °C, and the yield of products in a three-step torrefaction model [18]. This model was able to accurately predict the amount of various chemical species evolved during torrefaction and was based on the degradation of the hemicellulose material at 300 °C. The reaction model is shown below.

$$H \xrightarrow{k_1} R_1 + \sum_i \alpha_i P_i \tag{1}$$

$$R_1 \xrightarrow{k_2} R_2 + \sum_i \beta_i P_i \tag{2}$$

$$R_2 \xrightarrow{k_3} C + \sum_i \gamma_i P_i \tag{3}$$

In this model the initial hemicellulose (H) is degraded with reaction rate constant k_1 into a reaction intermediate R_1 and forms a suite of products $\{P_{i,1}\}$. The first reaction intermediate R_1 is then degraded with rate constant k_2 into a second reaction intermediate R_2 and produces more of these products $\{P_{i,2}\}$. The second reaction intermediate is then degraded with rate constant k_3 into the biocoal product (C) along with an additional release of reaction products $\{P_{i,3}\}$. This model accounts for the production of major torrefaction products through characteristic mass spectrometer (MS) ion fragments of: water (18 m/z), carbon monoxide (28 m/z), formic acid (29 m/z), carbon dioxide (44 m/z), acetic acid (60 m/z) and furfural (95 m/z).

This paper aims to deepen this model by applying this model over a range of torrefaction temperatures, and investigate the kinetics of torrefaction purely on the gas-phase reactions. In this work we take a lumped parameter assumption, where that the reaction rate coefficients are the same for each compound evolved, but the intensities of the specific species change with a stoichiometric coefficient (α,β,γ). These coefficients represent a relative amount of volatile product generated from each consecutive reaction stage, and are unique for each species—each of the six compounds investigated have a stoicheometeric parameter for each reaction. If this model is valid over the temperature range, then the stoichiometric coefficients should be independent of temperature for each of Eqs. (1)–(3). This assumption was validated in this research. This approach to predicting torrefaction is novel, but was previously investigated at only at 300 °C [18]. By obtaining gas-phase kinetics, accurate predictions of the volatile yields can be obtained for both isothermal and non-isothermal conditions. The dynamic evolution of these species was investigated, and unique implications of interpreting torrefaction through weight loss data in the absence of these novel results is discussed.

2. Materials and methods

As in our previous study [18] we used aspen biomass for this current research. Aspen samples were debarked then dried in an oven at 105 °C until no difference in mass was observed. A Thomas Wiley® knife mill (NR. 3557524 359264) was used to reduce the size of the wood particles. To obtain particle sizes of 0.5–0.6 mm a W.S. Tyler Rotap (model RX-29, serial 9774) was used. The aspen samples were roughly cylindrical with diameters of approximately 0.5 mm and length ranging from 1 to 3 mm.

2.1. Torrefaction experiments

To obtain kinetic data, the dried aspen wood samples were torrefied using a CDS Analytical micro-pyrolysis unit (model 5200HP Pyroprobe). The aspen was torrefied at temperatures of 260 °C to 300 °C at 10 °C intervals for 90 min. The volatile species evolved were continuously analyzed using a Trace GC Ultra (Model K8880181) gas chromatograph by ThermoFisher and a quadrupole mass spectrometer (Trace DSQII, ThermoFisher). The GC was fit with an inert, non-retentive, 10 m fused silica column (Restek, Rxi Guard Column). This eliminated any interaction with the compounds in the GC, and acted as a transfer line from the torrefaction reactor to the MS.

Aspen samples of 0.1–0.2 mg were weighed to within an accuracy of 1 μg using a microbalance (Citizen Scales Inc., Model CM5). The samples were then placed in a quartz reaction tube (25 mm × 2 mm OD) and held in place by two small pieces of glass wool on either end of the reaction tube. The samples were loaded into the micro-pyrolysis unit such that the wood chips were within the center of the heating zone and rapidly heated to the desired temperature. Rapid heating (1000 °C/s) was accomplished using a platinum heating filament that surrounded the quartz reaction tube. Ultra high purity helium (99.999%) was used as the carrier gas in order to create an inert atmosphere within the reaction zone and to transport the gaseous and vapor products into the inlet port of the GC through a heated stainless steel transfer line (300 °C). The GC column was kept at 300 °C for all experiments and the flow of helium gas kept at 1.5 ml/min (superficial velocity of 50.9 cm/s). After the samples passed through the GC, they then entered the quadrupole mass spectrometer where the ion fragments' intensities with respect to time were recorded. The mass spectrometer measured the continuous signal of ions from 15 to 350 m/z for 90 min. Data were then exported to a Microsoft Excel sheet for analysis. The measured data were normalized by dividing the MS intensity measured at each time point by the initial mass of aspen.

2.2. Model fitting

As mentioned, the proposed model (Eqs. (1)–(3)) is a consecutive 3-step degradation model for the early stages of torrefaction (up to 90 min). This model was developed for the main products from torrefaction: CO, CO_2, H_2O, organic acids (acetic acid and formic acid), and furfural [9,18,23] (although some studies report that methanol, methane, formaldehyde, and hydrogen are also observed [9,23–29], they were excluded here because they were not formed in any detectable level in our studies). Measuring these compounds over the course of torrefaction can yield information about the gas phase formation kinetics. In addition, changes in recalcitrance of the torrefied biomass, and changes in elemental composition can be inferred.

From our previous study [18] it was shown that at early times the production rate from Eq. (1) is dominant, while at later times Eq. (3) is the most important for product formation. An estimate for the parameters in Eq. (1) ($H_0\alpha_i$, k_1) during early time (0.5–2.0 min) and the parameters for Eq. (3) ($H_0\gamma_i$, k_3) at late times (>60 min) were obtained by adjusting the parameters to match the production intensity (stoichiometric coefficients) and dynamics (rate constants) over the specified times. The final parameters for Eq. (2) ($H_0\beta_i$, k_2) were then fit using a nonlinear, generalized reduced gradient method. The fitting routine was performed in Microsoft Excel around reducing the sum of squared error between the model and all measured data.

This method assumes that torrefaction is a set of devolatilization reactions that take place over a range of temperatures. Further, this implies that the stoichiometric parameters (α, β, γ) are independent of temperature. In addition, the model predicts lumped groups of product formation (i.e. all species have the same rate constant for each reaction step). These assumptions in the formation of the model are important and yield constraints about the system, and chemical significance. Because the same reactions are assumed to occur over the temperature range, a constraint is imposed that the stoichiometric parameters should not deviate with temperature. Validation of this is investigated in a following section. Further, the kinetics of torrefaction have been shown to closely follow traditional Arrhenius behavior [10,11,15–17,22,28,30,31] and impart further insight into kinetic aspects of the modeling. Initial estimates for the rate constants described above were used to obtain an initial set of Arrhenius parameters. These values were then used to obtain a new set of rate constants that are strictly linear on a $\ln k$ vs. $1/T$ basis. These values were then allowed to change along with the stoichiometric parameters (α, β, γ) in the iterative process of reducing the sum of squared error between the model and the experimental data. This method was followed for all species and temperatures.

All six volatile species were examined over the temperature range of 260–300 °C, however, when the torrefaction temperature decreased to 260 °C, carbon monoxide was not generated in sufficient quantity to produce a clear signal in the detector. A very low signal to noise ratio (S/N) makes it impossible to distinguish from the background noise, and these data were therefore excluded from the set.

3. Results and discussion

3.1. Experimental and modeling results

Fig. 1 shows typical traces of all compounds at 20 °C intervals (to simplify the presentation) to demonstrate the different behaviors observed in the formation of gaseous and vapor products. Remaining data traces are shown in the supplemental materials. These traces are directly related to the rates at which these components are produced. The figure also shows that as the temperature increases, the characteristic reaction times decrease. At early times, during the initial decay, we can observe the highest intensities for the products at the highest temperatures. As the temperatures decrease these production rates slow, and the production is prolonged over later times. This behavior flattens out the production curves, and thus demands much longer times to reach the same production amounts. From the figure, the steady decrease in production rate with temperature is intuitive and suggests simple temperature dependence. The production rate data decrease significantly over the 40 °C investigation range. This suggests that the process is very sensitive to both temperature and time, and any relative decrease in temperature would require a much longer processing time to reach the same feedstock degradation.

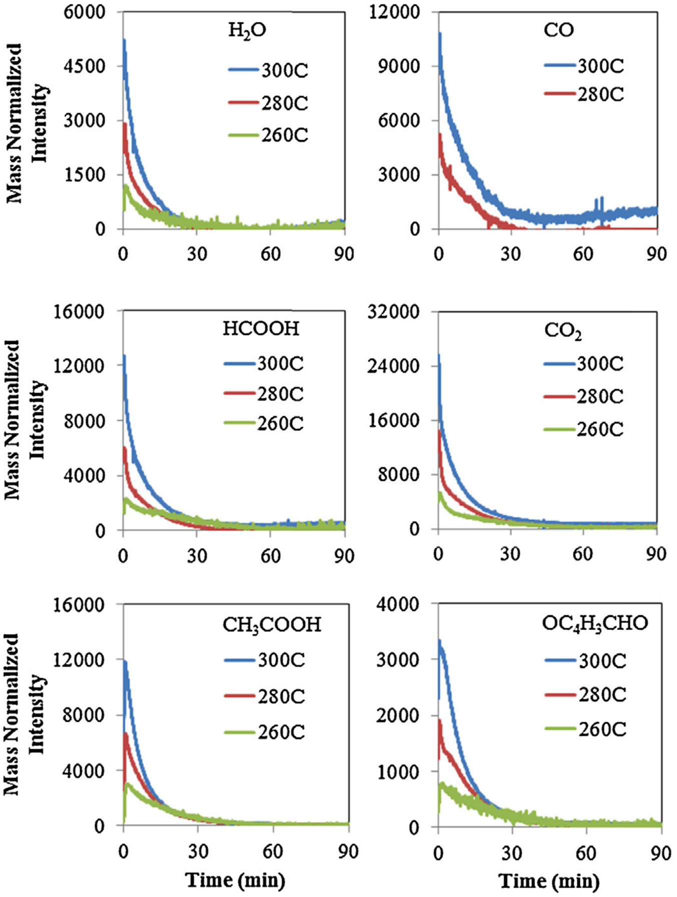

Fig. 1. Experimental transient trends for 18 m/z (H_2O), 28 m/z (CO), 29 m/z (HCOOH), 44 m/z (CO_2), and 60 m/z (CH_3COOH), and 95 m/z (OC_4H_3CHO) at varying temperatures.

Except for very early times, all compounds appear as a monotonic decay that decreases with decreasing temperature, but require several reactions to describe both the early and late time production rates. The acetic acid and furfural behavior is more complicated, and exhibits a slightly delayed production. These compounds are dominated by a delayed apex production peak shortly after the initial rate. The modeling of these traces, as shown in Fig. 2, demonstrates that the initial monotonic production (Eq. (1)) of acetic acid and furfural is quickly overtaken by a larger production in the subsequent reactions (Eqs. (2) and (3)). This generates a production apex after the initial time. Like the other traces, this peak decreases in size with decreasing temperature as

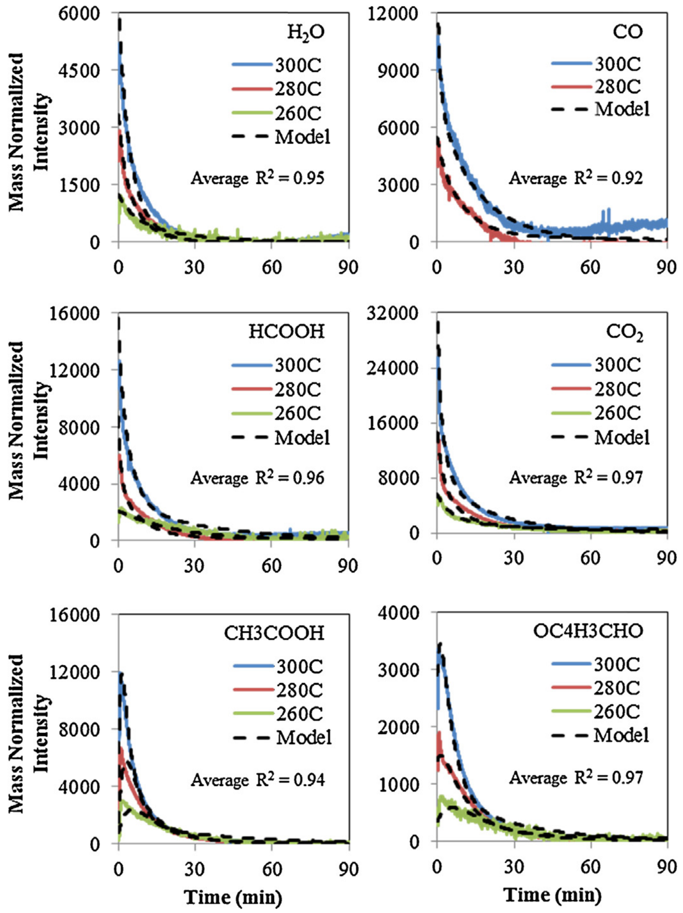

Fig. 2. Model fitting for all compounds at different torrefaction temperatures. The experimental data are shown as solid lines. The model at each temperature is shown as dashed lines.

the production delayed in time enough that it is masked by the slow kinetics. Fig. 2 shows typical model fits for all six compounds at 20 °C intervals. Good agreement between the model and the recorded data was observed over the temperature range investigated. Remaining transient sets are displayed in the supplemental section.

3.2. *Model validation*

It is important to note, again, that the model was assumed to apply over the whole temperature range—meaning the stoichiometric coefficients (α, β, γ) should be independent of temperature. In addition, the rate coefficients are species independent - meaning the model predicts lumped groups of product formation. The kinetic parameters were fit to the experimental data as explained above and for α, β, and γ. To examine the variability in these stoichiometry parameters, the average value of α determined for all species and temperatures, and α/α_{avg} was plotted as a function of temperature. These results are shown in Fig. 3. The figure shows the scatter in values for α away from the average. Although there is some variability, the value is approximately constant with temperature. Similarly the contribution from (Eq. (2)) and (Eq. (3)) were investigated as functions of temperature, and in relation to the production from (Eq. (1)) through α. Fig. 4 shows values for β/α and γ/α over the experimental temperature range, again supporting that the values are temperature independent. These confirming aspects of this work can lead to further chemical insight and development from a lumped product model to a more detailed reaction degradation mechanism. In conclusion, all values obtained for α/α_{avg}, β/α and γ/α validated that the stoichiometric coefficients are temperature independent, because we are dealing with the same reactions.

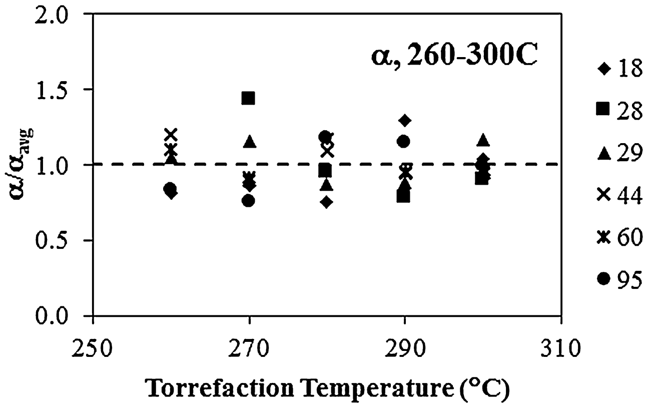

Fig. 3. Values of alpha for each component over 260–300 °C.

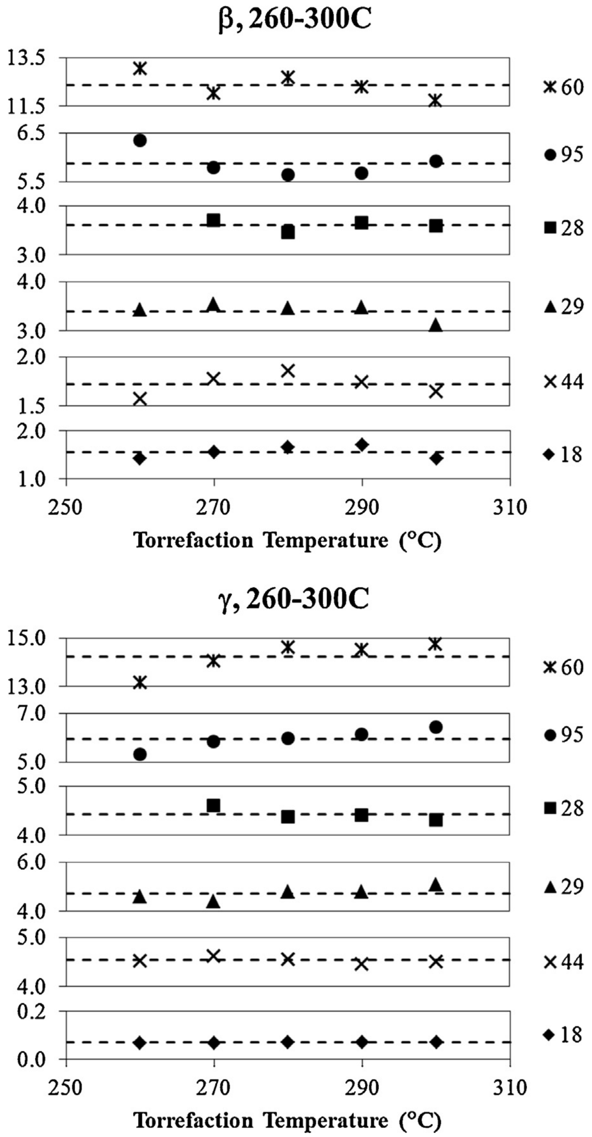

Fig. 4. Values for β (top) and γ (bottom) over 260–300 °C.

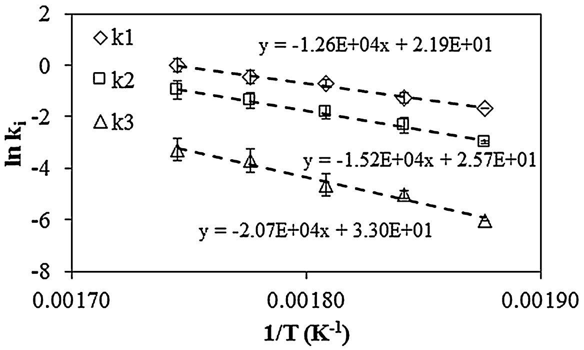

Fig. 5. Arrhenius plot for the three reaction model at 260–300 °C.

Table 1
Kinetic parameters for various feedstocks in a two-stage degradation scheme.

Feedstock	A1 (min^{-1})	A2 (min^{-1})	E1 (kJ/mol)	E2 (kJ/mol)	Source
Xylan	2.17E7	2.30E4	76.6	54.8	[17]
Beech	1.6 E6	3.6 E11	76	143	[27]
Straw	1.46E6	3.26E3	64.6	47.3	[30]
Corn stalks	3.78E8	1.62E5	91.5	65.2	[30]
Willow	1.49E6	6.6E11	76.0	151.7	[10,19]
Wheat straw	2.09E6	2.60E5	71.0	76.6	[24]

3.3. *Arrhenius parameters*

Fig. 5 shows the relationship between the three reaction rate constants (as obtained from our fitting procedure) and temperature. The error bars represent the standard deviation between the specific rate constant for all species at the specified temperature, showing very good agreement (with R^2 for the three trends 0.99, 0.99, and 0.98, respectively). These data collected from the chemical species model employed in this work show, as others have with only weight loss curves, that the kinetics of torrefaction closely follow Arrhenius behavior [10,11,15–17,22,28,30,31]. The pre-exponential factors are 3.32E9, 1.43E11, and 2.08E14 min^{-1}, respectively. The activation energies are 1.05E2, 1.27E2, and 1.72E2 kJ/mol, respectively. This Arrhenius behavior demonstrates that the three reaction model is able to capture the temperature dynamics quite well. These kinetic parameters can be used to predict changes in rates at reaction conditions and hence control the torrefaction process and its product distribution.

The proposed model assumes that each reaction produces a group of products through a lumped kinetic rate constant, or, the unique reaction rate constant is responsible for production of all species in that reaction step. The determined kinetic parameters, then, are related to an equivalent scheme and parameters based on weight loss measurements. The two-stage Di Blasi and Lanzetta model [17] has been applied to different types of feedstock include xylans [17,20,30], woody feedstock [10,19,20,22,30,32], and straws [28,33]. Table 1 shows a summary of kinetic parameters for the various feedstock. The activation energies for the three stage Branca and Di Blasi model [21,22] were 76.2, 142.8, and 43.8 kJ mol^{-1}, respectively, and the pre-exponential factors were 2.69E4, 5.91E9, and 10.0 s^{-1} (1.6E6, 3.6E11, and 6.0E2 min^{-1}) respectively. While the present study predicts higher activation energies are required for decomposition and a progressively more recalcitrant solid structure as torrefaction progresses, the overall magnitude of the parameters are similar, and should differ with biomass source.

Over the temperatures and duration of torrefaction studied, the present work has reasonably predicted the product formation of the six major gas/vapor products. This accounts for any changes, by difference, in the torrefied biomass. In addition to accurately predict the observed experimental data, the predicted kinetics are repeatable and closely follow traditional Arrhenius behavior. The observed energies have a similar magnitude to values that others have obtained with similar weight-loss schemes discussed above. The activation energies proposed in this work predict that at early times the biomass structure is relatively easily broken down compared to Eqs. (2) and (3). As torrefaction progresses, however, the subsequent reaction steps require more energy. This increase from Eq. (1) to Eq. (2), and from Eq. (2) to Eq. (3) implies that the solid intermediates are becoming progressively more recalcitrant with torrefaction severity. Heat and mass transfer effects have been shown to be negligible in previous work [18]. Therefore, the instantaneous heating rates employed are able to decrease any impacts or complications of heat ramping involved in prior TGA methods. Finally, the modeling of experimental data supports our assertion that the same global reactions are taking place over the range of torrefaction temperatures—or that the stoichiometric ratios of product formation are independent of temperature.

Table 2
Relative stoichiometric coefficients produced from reaction one (α), two (β), and three (γ) ±one standard deviation.

Compound	α, Unity	β, Norm	γ, Norm
H_2O	1.0 ± 0.2	1.6 ± 0.1	0.1 ± 0.0
CO	1.0 ± 0.3	3.6 ± 0.1	4.4 ± 0.1
CO_2	1.0 ± 0.1	1.7 ± 0.1	4.5 ± 0.1
HCOOH	1.0 ± 0.1	3.4 ± 0.2	4.7 ± 0.3
CH_3COOH	1.0 ± 0.1	12.0 ± 0.5	14.0 ± 0.7
OC_4H_3CHO	1.0 ± 0.2	5.9 ± 0.3	6.0 ± 0.4

3.4. *Reaction contributions in product profiles*

The stoichiometric coefficients obtained from our work provide a way to compare the production contributions from each reaction step. Note that the coefficients in the above mechanism are specific to each component, but independent of temperature. To more readily compare these coefficients, they are normalized to the amount of product formed from Eq. (1). These relative contributions are shown in Table 2. As can be seen from the table, the majority of water is produced from the first ($\alpha = 1$) and second ($\beta/\alpha = 1.6$) reactions. Very little production ($\gamma/\alpha = 0.1$) from the third reaction takes place at long times. In stark contrast to that, most compounds are only produced in significant quantities at later reaction times; for example acetic acid has small contribution from Eq. (1) ($\alpha = 1$), with a major contribution from Eq. (2) ($\beta/\alpha = 12.0$) and Eq. (3) ($\gamma/\alpha = 14.0$). This suggests that very careful consideration of torrefaction severity and duration is required to match the desired process outcomes with process conditions.

If these results are examined through the lens of an anticipated product distribution, the relationship between weight loss, product evolution, and product characteristics can be realized. It is known that the gas phase products are comprised mostly of water, acetic acid, and CO_2 (for example Ref. [9] indicated for willow the products are 89.3% water, 4.8% acetic acid, and 3.3% CO_2; other literature values are in the same magnitude but differ slightly with biomass source). Using our stoichiometric parameters and the product distribution of Ref. [9], the product evolution profiles were found and are shown in Fig. 6. If total weight loss is examined alone, it would appear that only a few minutes are required to complete the majority of the torrefaction process. However, an examination of the chemical species evolution reveals that long processing times are required to evolve carboxylic and other group compounds. Removal of these groups from the raw biomass is required for the biocoal to resemble the characteristics of fossil coal [3–7,34].

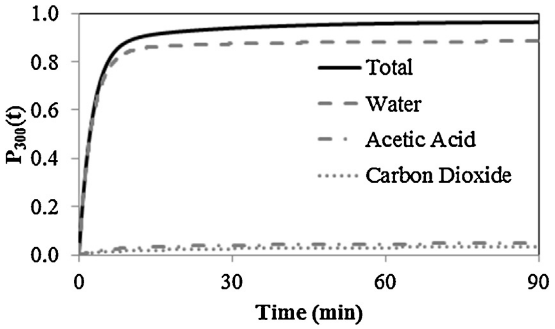

Fig. 6. Total product profiles for water, acetic acid and carbon dioxide with a product distribution.

Similar delayed feedstock decomposition and gaseous/vapor evolution profiles have been previously observed, but not modeled or extensively characterized [10,19,22,35]. It is our assertion here, and from our previous study [18], that while these late-time degradation steps may appear negligible from a weight loss viewpoint, they are an important consideration consisting of removing primary organics. These longer reaction times lead to preferable changes in torrefied biomass properties.

4. Conclusions

This study demonstrates that the three step model can accurately predict gas-phase product kinetics over the initial stages of torrefaction (up to 30% mass loss) from 260 to 300 °C. The pre-exponential factors obtained were 3.32E9, 1.43E11, and 2.08E14 min^{-1}, and the activation energies were 1.05E2, 1.27E2, and 1.72E2 kJ/mol for the three reactions, respectively. At early times, the evolution of chemically formed water dominates, while later times are required to remove the organic compounds such as acetic acid. Understanding torrefaction product evolution may lead to better prediction of product quality from varying or non-isothermal processing conditions, a topic to be investigated in future work.

Acknowledgements

The authors would like to gratefully acknowledge the National Science Foundation grant MPS/CHE—ENG/ECCS–1230803 for support of this work through a Sustainable Energy Pathways grant, and the Richard and Bonnie Robbins Endowment.

Appendix A. Supplementary data

Supplementary data associated with this article can be found, in the online version, at http://dx.doi.org/10.1016/j.jaap.2014.10.008.

References

[1] DOE/EIA, Report No.: DOE/EIA-0383, U.S. Energy Information Administration, 2014.
[2] EIA, Report No.: DOE/EIA-0383, EIA, 2010.
[3] D. Ciolkosz, R. Wallace, Biofuels, Bioprod. Biorefin. 5 (2011) 317.
[4] T.G. Bridgeman, J.M. Jones, A. Williams, D.J. Waldron, Fuel 89 (2010) 3911.
[5] P.C.A. Bergman, ECN Biomass, DEN programme of SenterNovem, in: Report ECN-C-05-073, Dutch Ministry of Economic Affairs, 2005.
[6] M.J.C. van der Stelt, H. Gerhauser, J.H.A. Kiel, K.J. Ptasinski, Biomass Bioenergy 35 (2011) 3748.
[7] J.J. Chew, V. Doshi, Renewable Sustainable Energy Rev. 15 (2011) 4212.
[8] H. Yang, R. Yan, H. Chen, D.H. Lee, C. Zheng, Fuel 86 (2007) 1781.
[9] R.D. Boardman, J.R. Hess, S. Sokhansanj, J.S. Tumuluru, C.T. Wright, Ind. Biotechnol. 7 (2011) 384+.
[10] M.J. Prins, K.J. Ptasinski, F.J.J.G. Janssen, J. Anal. Appl. Pyrolysis 77 (2006) 28.
[11] W.-H. Chen, P.-C. Kuo, Energy 36 (2011) 6451.
[12] L. Shang, J. Ahrenfeldt, J.K. Holm, A.R. Sanadi, S. Barsberg, T. Thomsen, W. Stelte, U.B. Henriksen, Biomass Bioenergy 40 (2012) 63.
[13] M. Phanphanich, S. Mani, Bioresour. Technol. 102 (2011) 1246.
[14] F. Shafizadeh, P.P.S. Chin, Wood Technology: Chemical Aspects, American Chemical Society, Washington, D.C., 1977, pp. 57, Chapter 5.
[15] V. Repellin, A. Govin, M. Rolland, R. Guyonnet, Biomass Bioenergy 34 (2010) 602.
[16] M. Broström, A. Nordin, L. Pommer, C. Branca, C. Di Blasi, J. Anal. Appl. Pyrolysis 96 (2012) 100.
[17] C. Di Blasi, M. Lanzetta, J. Anal. Appl. Pyrolysis 40–41 (1997) 287.
[18] J. Klinger, E. Bar-Ziv, D. Shonnard, J. Anal. Appl. Pyrolysis 104 (2013) 146.
[19] R.B. Bates, A.F. Ghoniem, Bioresour. Technol. 124 (2012) 460.
[20] T. Nocquet, C. Dupont, J.-M. Commandre, M. Grateau, S. Thiery, S. Salvador, Energy 72 (2014) 188.
[21] C. Di Blasi, C. Branca, F. Masotta, E. De Biase, Energy Fuels 27 (2013) 2665.
[22] C. Branca, C. Di Blasi, J. Anal. Appl. Pyrolysis 67 (2003) 207.
[23] M.J. Prins, K.J. Ptasinski, F.J.J.G. Janssen, J. Anal. Appl. Pyrolysis 77 (2006) 35.
[24] T. Nocquet, C. Dupont, J.-M. Commandre, M. Grateau, S. Thiery, S. Salvador, Energy 72 (2014) 180.
[25] C. Couhert, S. Salvador, J.M. Commandré, Fuel 88 (2009) 2286.
[26] J. Deng, G.-j. Wang, J.-h. Kuang, Y.-l. Zhang, Y.-h. Luo, J. Anal. Appl. Pyrolysis 86 (2009) 331.
[27] M. Pach, R. Zanziand, E. Björnbom, Sixth Asia-Pacific International Symposium on Combustion and Energy Utilization, Kuala Lumpur, Malaysia, 2002.
[28] L. Shang, J. Ahrenfeldt, J.K. Holm, S. Barsberg, R.-z. Zhang, Y.-h. Luo, H. Egsgaard, U.B. Henriksen, J. Anal. Appl. Pyrolysis 100 (2013) 145.
[29] Y. Chen, H. Yang, Q. Yang, H. Hao, B. Zhu, H. Chen, Bioresour. Technol. 156 (2014) 70.
[30] S. Cavagnol, E. Sanz, W. Nastoll, J.F. Roesler, V. Zymla, P. Perré, Thermochim. Acta 574 (2013) 1.
[31] A. Sarvaramini, G.P. Assima, F. Larachi, Chem. Eng. J. 229 (2013) 498.
[32] S. Ren, H. Lei, L. Wang, Q. Bu, S. Chen, J. Wu, Biosystems Eng. 116 (2013) 420.
[33] M. Lanzetta, C. Di Blasi, J. Anal. Appl. Pyrolysis 44 (1998) 181.
[34] A.J. Panshin, C. deZeeuw, Textbook of Wood Technology, McGraw-Hill Book Company, New York, NY, 1980.
[35] T.G. Bridgeman, J.M. Jones, I. Shield, P.T. Williams, Fuel 87 (2008) 844.